A Control-Oriented Model for Bead Cross-Sectional Geometry in Fused Deposition Modeling

Doruk Aksoy, Efe C. Balta, Dawn M. Tilbury, Kira Barton

***Abstract*— Additive manufacturing (AM) is a digital manufacturing technology that manufactures a 3D object in a bottom-up and layer-by-layer fashion. Fused deposition modeling (FDM), also known as desktop 3D printing, is one of the most commonly used AM technologies with numerous applications in academia and industry. Some of the greatest challenges with FDM include poor repeatability and reliability of the process, leading to mid-process failures or out-of-spec final products. Closed-loop control applications for FDM have been proposed as a means of mitigating mid-process failures. However, no models currently exist to enable control of the bead cross-sectional dimensions for the extruded material. This work presents a control-oriented model describing the effect of process parameters on cross-sectional dimensions of the deposited beads in FDM. A geometric model is presented and a procedure to evaluate the unknown machine and material specific parameters in the model is provided by leveraging design of experiments. The proposed model is experimentally validated and the accuracy of the results is presented. The results show that the proposed model accurately represents the bead cross-sectional geometry and is suitable for closed-loop control applications.**

I. Introduction

Additive manufacturing (AM) is a digital manufacturing process, in which a geometric design of a product is constructed by adding material layer-by-layer. AM allows for the manufacturing of complicated geometries with hollow or assembled structures in a single production step. Fused deposition modeling (FDM) is a subset of AM technologies in which a thermoplastic material is extruded through a numerically controlled extruder head to build a 3D geometry in a layer-by-layer fashion. Deposited thermoplastic beads have elliptical cross-sections [1] as demonstrated in Fig. 1.

Various applications of FDM are available both in academia and industry, [2], [3], [4]. Despite the widespread use for prototyping and production of customized products, reliability of FDM processes is an issue due to the open-loop nature of the deposition dynamics. In most of the current applications, an FDM deposition system is run by predefined inputs in open-loop that can lead to mid-print failures in the presence of disturbances. For high-performance applications with stringent specifications on the process parameters and tight tolerances on the dimensional accuracy of the end-products, efficient closed-loop controllers for FDM processes must be developed.

This work is supported by the National Science Foundation Grant #1544678, and NIST Award Nos. 70NANB16H205, 70NANB19H090.

Doruk Aksoy, Efe C. Balta, Dawn M. Tilbury, and Kira Barton are with the Department of Mechanical Engineering, University of Michigan, Ann Arbor, MI 48109 {doruk, baltaefe, tilbury, bartonkl} @umich.edu

A. Motivation and Problem Statement

While metal-based AM has been predominantly used in high-precision applications in current practice, FDM has been increasingly adopted due to its ease of use and low operational cost compared to the metal-based AM technologies. Medical applications of FDM are an important area that require high-precision end-products with accurate dimensional representations at reduced costs. FDM printed 3D models have been utilized as accurate anatomic templates in preparation for complicated surgical procedures in [5]. Customized prosthetics [6] and implants [7], [8] are another application area for FDM in medicine, where high geometrical precision and smooth surface finish are required for patient comfort and accurate healing.

There has been recent work on developing control and data analytics for FDM process dynamics to enable high-precision applications [9], [10], [11], [12]. However, a control-oriented model for adjusting the process parameters and compensating for mid-process geometrical inaccuracies in the deposited bead cross-sectional shape has yet to be devised.

B. Literature Review

There has been work on analyzing the deposition cross-sectional shape of additively manufactured parts, but little insight has been provided regarding the behavior of thermoplastic materials. In [13], authors analyze the bond width between the beads of subsequent layers using a custom made extruder equipped with inline pressure and temperature sensors, but provide no control-oriented model to estimate the bead cross-sectional shape from the FDM process parameters. There have been computational developments on modeling the cross-sectional geometry based on the process and material parameters [14]. While computational models describe the behavior of the deposited material in high-fidelity, these models are often computationally intensive and not readily suitable to be adapted in closed-loop control applications for in-situ process control.

In [11], a controller for synchronized material deposition rate and path velocity to reduce the deposition of excessive material at the sharp corners of the printed parts is proposed. In [15], load cells are integrated into FDM to determine the stiffness of the printed part and optimize the width of the printed part according to design. However, both [11] and [15] utilize fixed bead cross-sectional geometries in their models, and a model for adjusting the geometrical shape of the bead cross-sections is not provided. An example of in-situ metrology in FDM for bead geometry estimation

includes [16], where laser sensors are utilized in-situ heightmaps of the printed part during the printing p

There has been control work on AM technologies to FDM. In [17], a process control structure that de underfills and overfills to minimize the voids within a part in fused deposition of ceramics (FDC) is p In [18], a model of the deposited rod width onto a s for a micro-robotic deposition process is develope these models utilize deposition flow dynamics that cantly differ from the thermoplastic material flow d of FDM. Additionally, they do not capture the layer bonding phenomenon in FDM with thermoplastic als [13]. A model predictive controller is given in control the extrusion process in freeze-form extrusi cation (FEF), but a model to adjust the process parameters for different bead cross-sectional shapes is not provided.

Previous work from the authors includes a model of the spatial dynamics of the FDM process to represent the layer-to-layer height evolution and analyze layer-to-layer stability [9]. However, [9] assumes a simplified model with fixed aspect ratio for the relationship of the process input parameters and cross-sectional geometry. All of the aforementioned works in the literature have focused on many other aspects of control in FDM, yet there is not a control model of bead cross-sectional shape for FDM processes with thermoplastic materials. This gap poses an important challenge for implementing closed-loop controllers that adjust the spatial input to the process. To compensate for mid-process disturbances and increase the repeatability of the process, a control-oriented model is needed. To address this gap, this work presents a novel control-oriented model for controlling the cross-sectional shape of the deposited beads in the FDM process. The main contributions of this work are:

- A new control-oriented model to capture the relationship of cross-sectional geometry of deposited beads to process inputs such as material deposition rate and standoff height.
- A control-oriented model to characterize the height of the intersection between the beads of subsequent layers based on the proposed model.
- Validation and a preliminary benchmark study to show the effectiveness of the proposed model.

The remainder of the paper is structured as follows. Section II provides preliminary definitions and assumptions that are used in the paper. Section III presents the proposed control-oriented model with the necessary derivations and a methodology to experimentally estimate the system and material-specific constants in the model. Section IV presents a benchmark study to validate the accuracy of the proposed model when in comparison to a baseline model. Section V provides concluding remarks and future research directions.

II. Preliminaries

A. Dimensions Used in the Model

The model uses machine-specific dimensions such as d_i, which refers to the diameter of the opening at the tip of the nozzle, the outer diameter d_o, which refers to the outer diameter of the annulus shaped surface around the opening of the nozzle, and d_f the diameter of the filament used in the printing. These parameters cannot be changed without modifications on the machine and are therefore considered fixed dimensions.

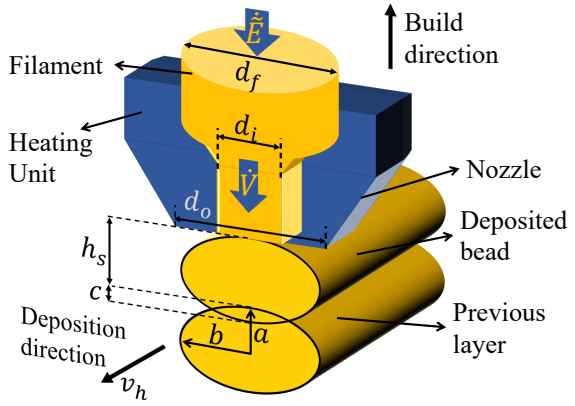

Fig. 1: Schematic of FDM deposition. a: minor axis of the ellipse, b: major axis of the ellipse, h_s: standoff height, c: interlayer bonding height, d_i: inner diameter of the nozzle tip, d_o: outer diameter of the nozzle tip, d_f: diameter of the filament, $\dot{V}$: volumetric material flow rate, $\dot{\tilde{E}}$: extrusion rate.

As shown in Fig. 1, the minor and major radii of the printed beads (a, b respectively), the inter-layer bonding height c, the standoff height of the nozzle tip h_s, the velocity of the extruder head v_h, the volumetric flow rate of the molten polymer $\dot{V}$, and the material feed rate into the extruder's melting chamber $\dot{\tilde{E}}$ are process-specific parameters of the proposed model. $\dot{\tilde{E}}$, v_h, and h_s are the inputs and the cross-sectional parameters a, b, and c are the states of the deposition model. The goal of this model is to lay the foundations for a control scheme such that $\left\|[a_r, b_r, c_r]^T - [a, b, c]^T\right\| \to 0$ can be achieved for a deposited bead, where the subscript r denotes reference values.

B. Assumptions

A list of standing assumptions used in deriving the proposed model in this work is listed here.

Assumption 1. *The volumetric flow rate of the material entering and exiting the extruder is conserved, i.e* $\dot{V}_{in} = \dot{V}_{extr}$.

This assumption ensures that the volume of material in and out of the extuder is conserved, enabling us to draw conclusions about the input $\dot{\tilde{E}}$ to bead area output. Based on this assumption, the value of $\dot{V}_{extr}$ is determined by the input $\dot{\tilde{E}}$, which we denote as the extrusion rate for the rest of the paper.

Assumption 2. *The tip of the nozzle remains in contact with the deposited layer.*

As extrudate is deposited, the extrusion rate $\dot{\tilde{E}}$ is used to control the cross-sectional area of the bead that has been

deposited at the standoff height h_s. To control the elliptical shape of the bead, a second geometrical constraint has to be set, which in this case is the standoff height of the nozzle.

While the height of the deposited bead is constrained as described in Assumption 2, the width of the deposited bead is constrained by the following assumption:

Assumption 3. *The width of the deposited bead (2b, see Fig. 1) does not exceed d_o*

This assumption is made to set an upper bound to $\dot{\bar{E}}$.

Assumption 4. *Material flow in the extruder is fully developed and in steady state.*

To be able to investigate the extruded material volume in a lumped fashion, the material flow in the extruder is considered to be fully developed.

Assumption 5. *The newly printed bead is deposited on the existing bead from the previous layer.*

The interaction between the base plate and the deposited bead is not investigated in this paper.

Assumption 6. *There is a linear relationship between the major axis of the deposited bead, the minor axis of the deposited bead, and the standoff height.*

Assumption 6 is adopted on this preliminary work to investigate a simple model form. Nonlinear relationships (e.g. polynomial) may result in models with higher accuracy in future work.

Assumptions 1, 4, and 5 are common assumptions in FDM literature and are adopted in most practical applications. The rest of the assumptions are specific for the proposed model and are discussed throughout the paper.

C. Definitions

In this study, the following geometrical properties are defined and used throughout the derivation of the model. The inter-layer bonding height c is defined as the height of the overlapping zone between two adjacent beads and given by $c = 2a - h_s$.

The parameter $k_{\dot{E}}$ is a multiplier for the minimum admissible extrusion rate $\dot{E}_{min}$ defined according to Assumption 2, which will be discussed in the following sections in detail. The bounds of $k_{\dot{E}}$ are determined so that the system is always in compliance with Assumptions 2 and 3.

III. Control-Oriented Bead Shape Model

A. Model derivation

Using Assumption 1 with $\dot{V}_{in} = \dot{V}_{extr}$, where $\dot{V}_{in} = \pi d_f^2 \dot{\bar{E}}/4$ and $\dot{V}_{extr} = \pi ab v_h$, the relationship between the extrusion rate ($\dot{\bar{E}}$) and the minor axis of the ellipse (a) can be given by (1)

$$\frac{d_f^2}{4v_h}\dot{\bar{E}} = ab. \tag{1}$$

The linear relationship in Assumption 6 is given by the following equation:

$$b = k_1 a + k_2 h_s. \tag{2}$$

where k_1 and k_2 are parameters that are characteristic to a given FDM printer. An experimental procedure to identify the coefficients k_1 and k_2 is discussed in the following sections. By leveraging (2), the value of b is substituted to derive the following relationship:

$$\frac{d_f^2}{4v_h}\dot{\bar{E}} = a(k_1 a + k_2 h_s). \tag{3}$$

The expression on the right hand side in (3) is converted into a quadratic expression so that a direct relationship between a and $\dot{\bar{E}}$ can be evaluated

$$k_1 a^2 + k_2 h_s a = \left(\sqrt{k_1}a + \frac{k_2 h_s}{2\sqrt{k_1}}\right)^2 - \frac{k_2^2 h_s^2}{4k_1}, \tag{4}$$

$$\dot{\bar{E}}\frac{d_f^2}{4v_h} + \frac{k_2^2 h_s^2}{4k_1} = \left(\sqrt{k_1}a + \frac{k_2 h_s}{2\sqrt{k_1}}\right)^2, \tag{5}$$

$$a = \left|\frac{k_2}{2k_1}\right| \sqrt{\frac{d_f^2 k_1}{k_2^2 v_h}\dot{\bar{E}} + h_s^2} - \frac{k_2 h_s}{2k_1}. \tag{6}$$

Substituting a given in (6) into (2) we obtain:

$$b = \left|\frac{k_2}{2}\right| \sqrt{\frac{d_f^2 k_1}{k_2^2 v_h}\dot{\bar{E}} + h_s^2} + \frac{k_2 h_s}{2}. \tag{7}$$

Since c is defined as $2a - h_s$ the resulting relationship is:

$$c = \left|\frac{k_2}{k_1}\right| \sqrt{\frac{d_f^2 k_1}{k_2^2 v_h}\dot{\bar{E}} + h_s^2} - \frac{(k_2 + k_1)}{k_1} h_s. \tag{8}$$

With the introduction of (8), expressions for all of the bead cross-section parameters a, b, c have been derived. To ensure Assumptions 2 and 3 hold, lower and upper bounds to an extrusion rate, $\dot{E}_{min}$ and $\dot{E}_{max}$ respectively, need to be determined.

To ensure contact with the tip of the nozzle, the height of the deposited bead needs to be greater or equal to half of the standoff height. There is also a material specific constant ϵ_1 that shifts this inequality due to the layer-to-layer bonding of the beads in subsequent layers; therefore:

$$a \geq \frac{h_s}{2} + \epsilon_1. \tag{9}$$

By using the lower bound on a from (9) and substituting into (6) after rearranging for $\dot{\bar{E}}$, we get the expression

$$\dot{E}_{min}(h_s, \epsilon_1) = \frac{4v_h k_1}{d_f^2}\left[\left[\frac{h_s}{2} + \epsilon_1 + \frac{k_2 h_s}{2k_1}\right]^2 - \frac{k_2^2 h_s^2}{4k_1}\right]. \tag{10}$$

In order to determine the upper bound for the extrusion rate $\dot{E}_{max}$, we first rearrange (7) for $\dot{E}(b, h_s)$ and substitute the following bound on b to ensure that the width of the

deposited material does not exceed the outer diameter of the nozzle tip:

$$b \leq \frac{d_o}{2} - \epsilon_2, \tag{11}$$

where ϵ_2 is a material specific coefficient to account for die swelling of the material upon extrusion [20]. Substituting the upper-bound on b from (11), we get the expression for $\dot{E}_{max}$

$$\dot{E}_{max}(h_s, \epsilon_2) = \frac{k_2^2 v_h}{d_f^2 k_1} \left[\frac{(d_o - 2\epsilon_2 - k_2 h_s)^2}{k_2^2} - h_s^2 \right]. \tag{12}$$

Beyond this point, $\dot{\tilde{E}}$ is considered to be comprised of the minimum extrusion rate ($\dot{E}_{min}(h_s, \epsilon_1)$) and the extrusion multiplier ($k_{\dot{E}}$). Any modifications to the extrusion rate $\dot{\tilde{E}}$ are achieved by modifying the extrusion multiplier $k_{\dot{E}}$, resulting in the following:

$$a = f(k_{\dot{E}} \dot{E}_{min}(h_s, \epsilon_1), h_s) = \left| \frac{k_2}{2k_1} \right| \sqrt{\frac{d_f^2 k_1}{k_2^2 v_h} k_{\dot{E}} \dot{E}_{min}(h_s, \epsilon_1) + h_s^2} - \frac{k_2 h_s}{2k_1}. \tag{13}$$

With this proposed model, the dimensions of the printed beads can be adjusted by modifying the extrusion multiplier ($k_{\dot{E}}$) at fixed standoff heights (h_s). To comply with Assumptions 2 and 3, the extrusion multiplier ($k_{\dot{E}}$) has to satisfy the inequality $1 \leq k_{\dot{E}} \leq \frac{\dot{E}_{max}}{\dot{E}_{min}}$, which maps to the feasible region depicted in Fig. 2. Note that to simplify the parameter estimation in this preliminary work, we use a fixed deposition velocity v_h and develop a model to capture the relationship between $\dot{\tilde{E}}$ and h_s.

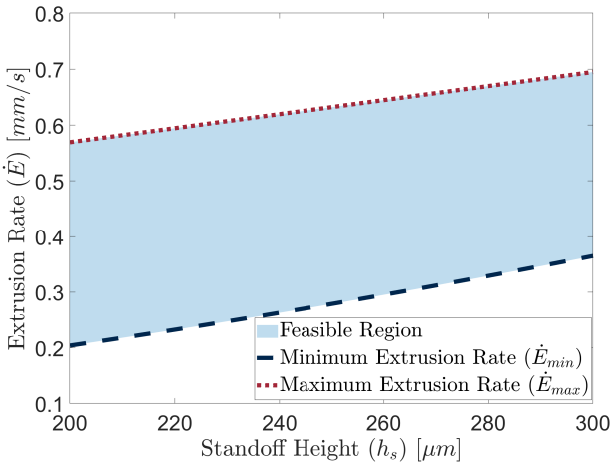

Fig. 2: Visualisation of the feasible extrusion rate region with bounds $\dot{E}_{min}$ and $\dot{E}_{max}$.

B. Parameter Estimation

There are material-specific (ϵ_1, ϵ_2) and system-specific parameters (k_1, k_2) that need to be determined. By selecting 3 different standoff heights and printing 3 specimens with different extrusion rates complying with Assumption 2, the system-specific constants are determined. Once the system-specific parameters are derived, material-specific parameters ϵ_1, ϵ_2 are searched for experimentally and the feasible region of the control-oriented model is evaluated (given by equations (9) and (11)). Using the system and material-specific parameters, upper and lower bounds for the extrusion rate ($\dot{E}_{min}(h_s, \epsilon_1)$ and $\dot{E}_{max}(h_s, \epsilon_2)$) are evaluated, in Fig. 2.

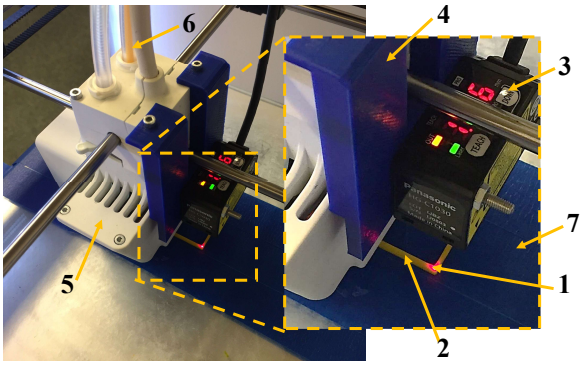

Fig. 3: Experimental setup for the case study. **1** - laser measurement point, **2** - square shell build geometry, **3** - laser distance measurement sensor, **4** - mounting piece for the sensor, **5** - extruder head of the FDM printer, **6** - PLA filament used in the experiment, **7** - heated build plate with the painters tape.

While printing the specimens for the experiments presented in this paper, a *Panasonic HG-C1030* laser distance sensor is used to collect in-situ layer height data to ensure that Assumption 2 holds during printing. The setup shown in Fig. 3 is used for the in-situ measurements. The laser distance sensor is mounted on the extruder head with a custom sensor mount, resulting in a finite spatial offset between the extruder tip and the measuring point of the sensor. The build plate is partially covered with painters tape to reduce measurement noise caused by the glare from the metal plate underneath the glass build plate. An *Arduino Mega 2560* is used as the data acquisition system. Compliance of the printed sample with Assumption 2, which is crucial for the feasibility of the proposed model, is checked by post-processing of the in-situ laser measurement data using MATLAB. To get in-situ height measurements of the printed beads in each layer, the experimental setup switches to measurement mode and the laser scanner measures the height of the most recently printed layer immediately after printing one layer of the specimen. To maintain material flow in the extruder as steady as possible and prevent any material flow flaws in the specimens, the extruder continues depositing material in the measurement mode as well, resulting in sacrificial rectangles printed at an offset from the actual specimen matching the offset between the tip of the nozzle and the measurement point of the laser. After the setup completes printing, the sacrificial rectangles are discarded.

1) Design of experiments

The proposed model is prepared for the range of $200 - 300$ μm standoff height that is standard in many commer-

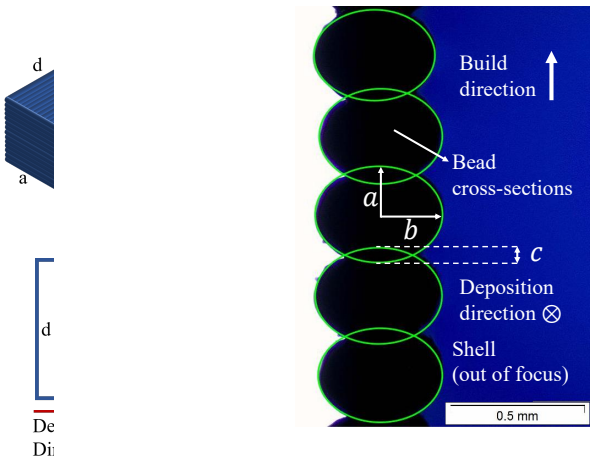

(i) (ii)

Fig. 4: (i) - Representative images of isometric (top) and top views (bottom) of a printed specimen (ii) - Real image of the A-A cross-section during the inspection process under *Olympus* digital microscope (5/12 of investigated layers visible).

cially available FDM printers. The experiments are conducted for the aforementioned standoff height range at three levels by keeping the same deposition velocity v_h. To be able to observe the effect of the extrusion rate $\dot{E}$, a base extrusion rate is chosen for each standoff height (in compliance with Assumption 2) and the extrusion multiplier $k_{\dot{E}}$ is altered between $1-2\times$ at three levels. By conducting a 2-factorial 3-level experiment, a mesh with $3^2 = 9$ points is experimentally obtained and used for plane fitting. For the experimental procedure, a 20-layer rectangular shell geometry having 20 mm width and 20 mm length is printed at $v_h = 20\ mm/s$ using blue PLA (PolyLactic Acid) from Ultimaker© ($d_f = 2850\mu m$). For each experiment, 2 sample prints with the same standoff height and extrusion rate are printed. After printing, the samples were cut (as shown in Fig. 4(i)) and an *Olympus* digital microscope was used to capture the cross-section images of the samples as shown in Fig. 4(ii). To get the bead dimensions, ellipses were manually fitted to the captured cross-sectional images in MATLAB.

The first 5 layers of each print are excluded from the analysis because of transient effects and material exuding from the nozzle during the dwell time between printing successive samples. Analysis of the material - build plate interactions [14] may help characterize the transient flow in the early layers, which is beyond the scope of this work. Starting from layer number 6, the minor and the major radii (a, b) of the layers $6-17$ are recorded and the mean values of the respective radii are reported as the result of each specific input combination. The selected base extrusion rates for standoff heights $200\mu m$, $250\mu m$, and $300\mu m$ are $0.218\ mm/s$, $0.296\ mm/s$, and $0.418\ mm/s$, respectively.

2) Results of the Experiments

Table I presents the results of the DOE experiments. The mean values for the radii are denoted with $\bar{a}$ and $\bar{b}$, for the minor and the major axes of the beads respectively, and the standard deviations of the experiment results from their respective mean values are denoted with $\sigma_{\bar{a}}, \sigma_{\bar{b}}$. Note that the significant figures of mean and standard deviation denote the statistical variation but do not correspond to the sensitivity of the experimental setup $(10\mu m)$.

TABLE I: List of DOE experiments and their results

Experiment #	$k_{\dot{E}}$	h_s $[\mu m]$	$\bar{a} \pm \sigma_{\bar{a}}$ $[\mu m]$	$\bar{b} \pm \sigma_{\bar{b}}$ $[\mu m]$
1	1	200	122.5 ± 2.6	167.7 ± 5.4
2	1.5	200	142.3 ± 4.3	244.2 ± 4.4
3	2	200	162.3 ± 1.8	328.2 ± 5.7
4	1	250	143.8 ± 2.9	193.3 ± 2.3
5	1.5	250	169.6 ± 5.2	264.6 ± 5.8
6	2	250	184.7 ± 3.1	348.4 ± 5.0
7	1	300	177.3 ± 3.8	231.2 ± 6.0
8	1.5	300	197.3 ± 3.5	309.6 ± 9.0
9	2	300	226.7 ± 4.1	393.1 ± 6.0

Utilizing the values given in Table I, a surface is fitted to the data points using the `surffit.m` function from MATLAB. The system-specific constants k_1, k_2 are estimated as 3.606 and -1.347 respectively, therefore equation (2) is given as

$$b = 3.606a - 1.347h_s. \tag{14}$$

The R^2 value of the fit is 0.9729. The fitted plane along with the data points used in the fit is shown in Fig. 5.

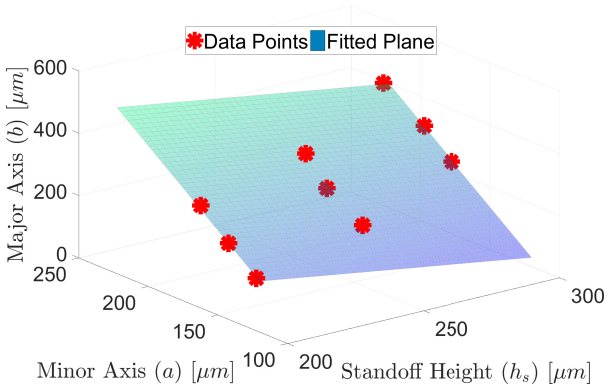

Fig. 5: Results of the experiments and the fitted surface for the model in Assumption 6, $b = k_1 a + k_2 h_s$ with $k_1 = 3.606$ and $k_2 = -1.347$. The R^2 value of the fit is 0.9729.

After obtaining the system-specific constants, the extrusion rate is increased from a known under-extruding value to obtain an approximation of the lower bound $\dot{E}_{min}$. While increasing the extrusion rate, the in-situ recorded height data is investigated to ensure that Assumption 2 holds. As a result of this procedure, the material-specific constant ϵ_1 is

determined as $\epsilon_1 = 21.864\mu m$, so that the lower bound from (9) becomes $a \geq 0.5h_s + 21.864\mu m$. Substituting this lower bound on a along with the system-specific constants k_1, k_2 into (10), the expression for the minimum extrusion rate becomes:

$$\dot{E}_{min}(h_s) = \frac{4v_h}{d_f^2}\left[\left[0.595h_s + 41.519\right]^2 - \frac{h_s^2}{7.950}\right]. \quad (15)$$

The same procedure is repeated for the upper bound, $\dot{E}_{max}$. This time the extrusion rate is decreased until the width of the printed shell geometry does not exceed the outer diameter of the nozzle tip $d_o = 1mm$ and therefore does not violate Assumption 3. Width of the printed parts were measured with a digital caliper. The material-specific constant ϵ_2 of the model is determined as $\epsilon_2 = 158.715\mu m$, such that the feasibility upper bound (11) becomes $b \leq 0.5d_o - 158.715$. Substituting this upper bound on b along with the system-specific constants k_1, k_2 into (12) the expression for the maximum extrusion rate becomes:

$$\dot{E}_{max}(h_s) = \frac{v_h}{1.987d_f^2}\left[\left(\frac{682.570 + 1.347h_s}{1.814}\right)^2 - h_s^2\right]. \quad (16)$$

After obtaining (15) and (16), the feasible extrusion rate region for the model can be depicted as in Fig. 2.

After obtaining the final expression for $\dot{E}_{min}$ given in (15), the equation is substituted back into (16) along with the system-specific constants k_1, k_2 determined from the experiments to give the final expression of the proposed model as the following.

$$a = f(k_{\dot{E}}, h_s) = \frac{1}{5.354}\left[h_s + \left(7.950k_{\dot{E}} \left[\left(0.595h_s + 41.519\right)^2 - \frac{h_s^2}{7.950}\right] + h_s^2\right)^{1/2}\right] \quad (17)$$

Using (14) and (17), an appropriate extrusion multiplier $k_{\dot{E}}$ (based on the minimum extrusion rate given by (15)) for a bead cross-section geometry with a desired standoff height (h_s) and bead major radius (b) may be evaluated.

IV. Model Validation

In this section, the proposed model is compared to a widely used cross-sectional shape estimation model in practice. A case study with an experimental procedure to compare the benchmark model to the proposed model is given and the results of the validation case study are presented.

A. Case Study

Computer aided design (CAD) files of product geometries are converted to machine commands (GCode) through *slicer* software. Slicer software takes cross-section cuts of the CAD model at predetermined height increments and converts the "sliced" geometry into GCode files, which contain the spatial commands for the 3D printers. The cross-sectional geometry estimation model used in a widely used slicing software *Slic3r*[1], can be seen in Fig. 6. The bead cross-section is modeled as a rectangle with two semi-circles at the ends. Using this method, the cross-sectional area can be modeled as $A_{Section} = A_{Rect} + A_{Circ} = wh_s + \pi(h_S/2)^2$. Furthermore, the required $\dot{E}$ is calculated as:

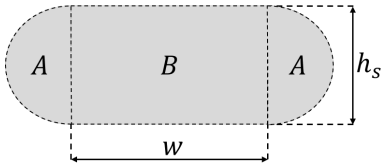

Fig. 6: Benchmark model for the bead dimension estimation. The deposited bead is approximated as a rectangle (B) with two half circles (A) on both ends. w: width of the rectangular section, h_s: standoff height.

$$\dot{E}_{bm} = \left(\frac{h_S^2\pi}{4} + h_s w\right)\frac{4v_h}{\pi d_f^2} \quad (18)$$

To test the performance of the proposed model, beads with varying reference dimension pairs (h_s $[\mu m], b$ $[\mu m]$) $= \{(230, 200),\ (270, 250),\ (290, 300)\}$ were printed. To achieve this, the extrusion rates for the benchmark model were determined as $\dot{E}_{bm} = \{0.253,\ 0.374,\ 0.489\}$ mm/s, respectively, using (18). Using (7) with the estimated parameters, the extrusion rates for the proposed model were determined as $\dot{E}_{pm} = \{0.279,\ 0.419,\ 0.566\}$ mm/s, respectively.

B. Validation

For model validation, two sets of experiments are performed with the calculated extrusion rates. The results of the benchmark study in terms of the mean major radii $(\bar{b})$ are presented in Table II.

As presented in Table II, the proposed model predicts the width of the printed bead with a maximum of 6.6% error,

TABLE II: Benchmark results of the case study

	h_s $[\mu m]$	$\dot{E}$ $[mm/s]$	$\bar{b} \pm \sigma_{\bar{b}}[\mu m]$	Error $\bar{b}$ [%]
Test 1				
Reference	230	—	200	—
Benchmark	230	0.253	169.0 ± 5.3	15.5
Proposed	230	0.279	187.7 ± 4.0	6.6
Test 2				
Reference	270	—	250	—
Benchmark	270	0.374	214.6 ± 3.2	14.2
Proposed	270	0.419	243.8 ± 4.3	2.5
Test 3				
Reference	290	—	300	—
Benchmark	290	0.489	258.4 ± 4.6	13.9
Proposed	290	0.566	293.8 ± 4.6	2.1

[1]https://manual.slic3r.org/advanced/flow-math

whereas the benchmark model estimates the bead width with a maximum of 15.5% error. From this case study, it is evident that the proposed model outperforms the benchmark model at estimating the width of the printed bead.

TABLE III: Estimation performance of the minor radii of the deposited beads

	$\dot{E}$ $[mm/s]$	a_{est} $[\mu m]$	$\bar{a} \pm \sigma_{\bar{a}}$ $[\mu m]$	Error $\bar{a}$ [%]
Test 1	0.279	141.3	143.7 ± 3.1	1.6
Test 2	0.419	170.2	170.6 ± 3.5	0.2
Test 3	0.566	191.5	196.3 ± 4.9	2.4

Since the benchmark model does not account for the inter-layer bonding height (c) and takes $h_s/2$ as the height of the layer, the performance of the proposed model is evaluated by comparing the estimated minor radii of the beads (a_{est}) calculated using (17) with the mean minor radii of the printed beads $(\bar{a})$. As it is shown in Table III, the proposed model predicts the minor radius of the printed beads with a maximum error of 2.4%.

TABLE IV: Estimation performance of the inter-layer bonding height

	$\dot{E}$ $[mm/s]$	c_{est} $[\mu m]$	$\bar{c} \pm \sigma_{\bar{c}}$ $[\mu m]$	Error $\bar{c}$ [%]
Test 1	0.279	52.8	60.9 ± 5.2	13.3
Test 2	0.419	70.3	75.0 ± 5.1	6.1
Test 3	0.566	93.0	104.6 ± 7.7	11.0

Furthermore, due to the lack of a model predicting the inter-layer bonding height (c), performance evaluation of the model is done by comparing the estimation of the proposed model for $c_{est}(\dot{E}, h_s)$, which is calculated by substituting (17) into $c = 2a - h_s$, with the mean inter-layer bonding height $(\bar{c})$ of the case study samples. The results of that comparison are presented in Table IV. The proposed model predicts the inter-layer bonding height with a maximum error of 13.3%.

V. Conclusion

Understanding the effect of process parameters on the cross-sectional geometry of deposited beads in FDM is crucial for closed-loop control applications. This work presents the first control-oriented model that quantitatively relates the standoff height and extrusion rate to the cross-sectional shape of the deposited beads. The inter-layer bond that is formed between beads is also modeled with high accuracy. The height of the inter-layer bond is an important parameter for FDM as it relates to the mechanical strength and surface roughness of the printed parts. The control-oriented model in this work provides a basis for implementing closed-loop control of for the spatial dynamics of FDM.

Future work will focus on utilizing the models provided in this work to develop and implement layer-to-layer closed-loop controllers for the spatial dynamics of FDM. Additionally, further studies to understand the limits of the feasibility regions for the proposed models are of interest. By utilizing the inter-layer bonding length, controllers to optimize part strength in FDM may be developed in the future.

References

[1] D. Ahn, J. H. Kweon, S. Kwon, J. Song, and S. Lee, "Representation of surface roughness in fused deposition modeling," *Journal of Materials Processing Technology*, 2009.

[2] C. Lunsford, G. Grindle, B. Salatin, and B. E. Dicianno, "Innovations with 3-dimensional printing in physical medicine and rehabilitation: a review of the literature," *PM&R*, vol. 8, no. 12, pp. 1201–1212, 2016.

[3] S. Kondor, G. Grant, P. Liacouras, J. R. Schmid, M. Parsons, V. K. Rastogi, L. S. Smith, B. Macy, B. Sabart, and C. Macedonia, "On demand additive manufacturing of a basic surgical kit," *Journal of Medical Devices, Transactions of the ASME*, vol. 7, no. 3, 7 2013.

[4] S. Gopakumar, "RP in medicine: A case study in cranial reconstructive surgery," *Rapid Prototyping Journal*, vol. 10, no. 3, pp. 207–211, 2004.

[5] J. R. Jastifer and P. A. Gustafson, "Three-Dimensional Printing and Surgical Simulation for Preoperative Planning of Deformity Correction in Foot and Ankle Surgery," *Journal of Foot and Ankle Surgery*, 2017.

[6] Y. H. Cha, K. H. Lee, H. J. Ryu, I. W. Joo, A. Seo, D. H. Kim, and S. J. Kim, "Ankle-foot orthosis made by 3D printing technique and automated design software," *Applied Bionics and Biomechanics*, vol. 2017, 2017.

[7] K. Moiduddin, S. Darwish, A. Al-Ahmari, S. ElWatidy, A. Mohammad, and W. Ameen, "Structural and mechanical characterization of custom design cranial implant created using additive manufacturing," *Electronic Journal of Biotechnology*, 2017.

[8] D. Bourell, D. Espalin, K. Arcaute, D. Rodriguez, F. Medina, M. Posner, and R. Wicker, "Fused deposition modeling of patientspecific polymethylmethacrylate implants," *Rapid Prototyping Journal*, vol. 16, no. 3, pp. 164–173, 4 2010.

[9] E. C. Balta, D. M. Tilbury, and K. Barton, "Control-oriented modeling and layer-to-layer stability for fused deposition modeling: a kernel basis approach," in *2019 American Control Conference (ACC)*. IEEE, 2019, pp. 4727–4733.

[10] ——, "A digital twin framework for performance monitoring and anomaly detection in fused deposition modeling," in *2019 IEEE 15th International Conference on Automation Science and Engineering (CASE)*. IEEE, 2019, pp. 823–829.

[11] D. S. Ertay, A. Yuen, and Y. Altintas, "Synchronized material deposition rate control with path velocity on fused filament fabrication machines," *Additive Manufacturing*, 2018.

[12] M. Duan, D. Yoon, and C. E. Okwudire, "A limited-preview filtered b-spline approach to tracking control–with application to vibration-induced error compensation of a 3d printer," *Mechatronics*, vol. 56, pp. 287–296, 2018.

[13] T. J. Coogan and D. O. Kazmer, "Modeling of interlayer contact and contact pressure during fused filament fabrication," *Journal of Rheology*, vol. 63, no. 4, pp. 655–672, 7 2019.

[14] R. Comminal, M. P. Serdeczny, D. B. Pedersen, and J. Spangenberg, "Numerical modeling of the strand deposition flow in extrusion-based additive manufacturing," *Additive Manufacturing*, vol. 20, pp. 68–76, 2018.

[15] K. Garanger, T. Khamvilai, and E. Feron, "Additive manufacturing for high precision structural properties via feedback control," Tech. Rep.

[16] L. Li, R. McGuan, P. Kavehpour, and R. Candler, "Precision enhancement of 3D printing via in situ metrology," in *Solid Freeform Fabrication 2018*, 2018, pp. 251–260.

[17] Y. Cheng and M. A. Jafari, "Vision-based online process control in manufacturing applications," *IEEE Transactions on Automation Science and Engineering*, vol. 5, no. 1, pp. 140–153, 1 2008.

[18] D. J. Hoelzle, A. G. Alleyne, and A. J. W. Johnson, "Iterative learning control for robotic deposition using machine vision," *2008 American Control Conference*, pp. 4541–4547, 2008.

[19] H. Zomorodi and R. G. Landers, "Extruison Based Additive Manufacturing Using Model Predictive Control," in *Proceedings of the American Control Conference*. Institute of Electrical and Electronics Engineers Inc., 2016, pp. 1747–1752.

[20] B. N. Turner, R. Strong, and S. A. Gold, "A review of melt extrusion additive manufacturing processes: I. Process design and modeling," *Rapid Prototyping Journal*, vol. 20, no. 3, pp. 192–204, 2014.